Available online at www.sciencedirect.com
SCIENCE DIRECT®
Earth and Planetary Science Letters 245 (2006) 595–604
EPSL
www.elsevier.com/locate/epsl

Quasi-geostrophic kinematic dynamos at low magnetic Prandtl number

Nathanael Schaeffer [1], Philippe Cardin *

LGIT, Observatoire de Grenoble, Université Joseph Fourier, and CNRS, BP 53, 38041 Grenoble cedex 9, France

Received 17 September 2005; received in revised form 27 January 2006; accepted 17 March 2006
Available online 2 May 2006
Editor: V. Courtillot

Abstract

Rapidly rotating spherical kinematic dynamos at very low Ekman and Prandtl numbers are computed using the combination of a quasi-geostrophic (QG) model for the velocity field and a classical spectral 3D code for the magnetic field. The QG flow is computed in the equatorial plane of the sphere; it corresponds to Rossby wave instabilities of a geostrophic internal shear layer produced by differential rotation. The induction equation is computed in the whole sphere after the QG flow has been expanded along the rotation axis. Differential rotation and Rossby wave propagation are the key ingredients of this dynamo which can be interpreted in terms of Parker-Ω dynamo. Taking into account the quasi-geostrophy of the velocity field enables us to increase time and space resolution to compute the dynamics. For the first time, we report on numerical dynamos with very low Ekman numbers (10^{-8}). Because the magnetic and velocity fields are computed on different grids, we compute dynamos for very low magnetic Prandtl numbers exhibiting a scale separation between magnetic and velocity field. These dynamos are asymptotically close to rapidly rotating, metallic planetary cores.

Keywords: kinematic dynamos; magnetic fields; geodynamo; geostrophy; quasi-geostrophic model; scale separation

1. Introduction

The magnetic field of the Earth is produced by dynamo action in the metallic liquid core of our rotating planet. Many efforts have been successfully made in the last decade to describe the mechanisms of self induced magnetic fields either with experimental models [1–3] or numerical simulations [4–7]. Both approaches have limitations. No experiment has been performed in rotation (except for one attempt with a precessional cylinder [8]) while rotation is seen as a key ingredient by geophysicists to explain the geometry and amplitude of the geomagnetic field [9]. All numerical models [10,11] have introduced Coriolis forces in the Navier–Stokes equation and the quasi-geostrophy (two dimensionality imposed by the Proudman–Taylor theorem [12]) of the flow plays a role in the generation of the magnetic field. Thermal convective vortices aligned with the rotation axis are associated to surface patches of magnetic field [7] and spatio-temporal behaviors of magnetic and vorticity fields are similar. This effect is a direct consequence of the prescribed magnetic Prandtl number ($P_m = \nu/\eta$, where ν is the kinematic viscosity and η the

* Corresponding author.
E-mail address: philippe.cardin@obs.ujf-grenoble.fr (P. Cardin).
[1] Present address: I.R.P.H.E., CNRS UMR 6594, 49, rue F. Joliot-Curie, BP 146, F-13384 Marsielle cedex 13, France.

0012-821X/$ - see front matter © 2006 Elsevier B.V. All rights reserved.
doi:10.1016/j.epsl.2006.03.024

magnetic diffusivity) in the simulations. The current computer capabilities limit the computations to magnetic Prandtl number of the order of unity [10] while liquid metals exhibit magnetic Prandtl numbers lower than 10^{-5}, even in planetary core conditions [13].

In this paper, we propose an approach aiming at computing very low magnetic Prandtl number dynamos taking advantage of the quasi-geostrophic behavior of the velocity field. For very low Ekman numbers ($E=\nu/\Omega R^2$, where Ω is the rotation rate of the spherical container, and R its radius), a quasi-geostrophic (QG) approach describes the flow correctly in a rapidly rotating sphere [14,15]. The flow equations are integrated along the direction of the rotation axis. Although the numerical variable is a stream function in the equatorial plane, the top and bottom boundary conditions are taken into account through the slope (β) and Ekman pumping effects. In the context of the study of thermal convection in rapidly rotating spherical shells, Aubert et al. [16] have successfully compared their QG results with 3D calculations [17] and experimental measurements [18].

Low values of P_m may imply a separation in terms of length-scales and frequencies, between the velocity and magnetic fields in a metallic dynamo. This idea has already been applied to kinematic dynamo computations at low P_m [19]. In this work, we compute the QG flow in the equatorial plane with a fine spatio-temporal resolution and the velocity is extrapolated to a coarse 3D spherical grid where the induction equation is solved.

In order to demonstrate the validity of this approach, we have decided to apply it to a simple case. Instead of a thermal convective flow for which heat transport has to be modeled, we consider the instabilities of an internal geostrophic shear layer. This layer, known as the Stewartson layer, is produced by a differentially rotating inner core in a rotating sphere and consists of two nested viscous shear layers [20,21]. Above a critical Ro number ($Ro=\Delta\Omega/\Omega$, where $\Delta\Omega$ is the differential rate of rotation of the inner core), the Stewartson layer becomes unstable [22] and generates Rossby waves [23].

The Geodynamo group in Grenoble is developing a spherical Couette liquid sodium experiment [24] in order to study magnetostrophic regime. Quasi-geostrophic numerical dynamos at low magnetic Prandtl numbers will help to better understand the experimental findings [25].

As we will show in this paper, such unstable flows can generate and sustain a magnetic field. The QG-model allows us to compute dynamos at very low Ekman (down to 10^{-8}) and magnetic Prandtl numbers (as low as 3×10^{-3}).

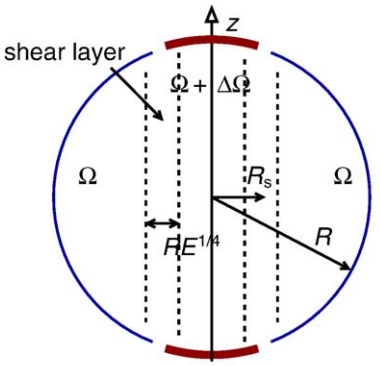

Fig. 1. Sketch of the split sphere geometry. The differential rotation produces an axisymmetric Stewartson $E^{1/4}$ shear layer which is cylindrical and aligned with the rotation axis z.

2. The equations

2.1. Hydrodynamics

Let us consider a sphere of radius R filled with an incompressible liquid metal of viscosity ν and magnetic diffusivity η. The sphere is rotating at along the z-axis of a cylindrical reference frame ($\mathbf{e_s}$, $\mathbf{e}_\phi$, $\mathbf{e_z}$). The sphere is split at the co-latitude $\pm\sin^{-1}(R_s/R)$ (R_s/R is set to 0.35). The two polar caps are rotating differentially at $\Omega+\Delta\Omega$ as shown in Fig. 1. Time, length and magnetic field will be scaled using Ω^{-1}, R, $(\mu_0\rho)^{1/2}R\Omega$, respectively. For low Ekman and Rossby numbers, the mainstream flow is quasi-geostrophic [12]. Taking the curl of the Navier–Stokes equation and averaging along the direction of the rotation axis z (denoted by an overbar), we get the QG equation for the z-component of the vorticity $\omega=\mathbf{e_z}\cdot\nabla\times\mathbf{u}$, provided that u_s and u_ϕ are independent of z [23].

$$\frac{\partial\omega}{\partial t}+u_s\frac{\partial\omega}{\partial s}+\frac{u_\phi}{s}\frac{\partial\omega}{\partial\phi}-(2+\omega)\frac{\overline{\mathrm{d}u_z}}{\mathrm{d}z}=\overline{[\nabla\times(\mathbf{j}\times\mathbf{B})]\cdot\mathbf{e_z}}+E\Delta\omega \quad (1)$$

The Coriolis term needs the evaluation of $\frac{\overline{\mathrm{d}u_z}}{\mathrm{d}z}$. We deduce that u_z is a linear function of z from the averaged mass conservation equation. Consequently, its vertical derivative may be deduced from the non penetration boundary condition (β effect) and the viscous boundary condition (the Ekman pumping effect) [23]:

$$\frac{\overline{\mathrm{d}u_z}}{\mathrm{d}z}=E^{1/2}P(u_s,u_\varphi,s)+\beta(s)u_s \quad (2)$$

where $\beta(s)\equiv\frac{1}{L}\frac{dL}{ds}|_{z=L}$ and $L(s)=\sqrt{1-s^2}$ is the half height of a column of fluid and

$$P(u_s,u_\varphi,s)=\frac{1}{2(1-s^2)^{3/4}}\times\left[-\omega+\frac{s}{1-s^2}\left(\frac{\partial u_s}{\partial\varphi}-\frac{1}{2}u_\varphi\right)-\frac{5s}{2(1-s^2)^{3/2}}u_s\right] \quad (3)$$

is the Ekman pumping boundary condition in a rigid sphere deduced from Greenspan's formula [23]. We would like to stress that this formula is applicable as long as all relevant time scales are much longer than the rotation period, which is a reasonable assumption for the small Rosby numbers considered in this study.

The axisymmetric flow is computed directly from the Navier–Stokes equation [26].

$$\frac{\partial\langle u_\phi\rangle}{\partial t}+\left\langle u_s\frac{\partial u_\phi}{\partial s}\right\rangle+\frac{\langle u_\phi u_s\rangle}{s}+2\langle u_s\rangle=\langle\overline{(\mathbf{j}\times\mathbf{B})}\cdot\mathbf{e}_\phi\rangle+E\left(\Delta\langle u_\phi\rangle-\frac{\langle u_\phi\rangle}{s^2}\right) \quad (4)$$

where $\langle\ \rangle$ stands for the ϕ-average operator. Rigid boundary conditions are assumed for the velocity at $s=1$. For $s<R_s/R$, the top and bottom azimuthal velocity are imposed as $u_\phi=sRo$. The velocity field is computed using a generalized stream function in the equatorial plane as in [23] which guarantees 3D mass conservation. The stream function is expanded in Fourier components along the ϕ component. It may be interesting to introduce the Reynolds number $Re=RoE^{-1}$ directly related to the two controlling dimensionless numbers E and Ro.

In this paper, as a first step, we will only consider kinematic dynamos and the magnetic terms in (1) and (4) will be neglected.

2.2. Induction equation

The velocity field computed with Eqs. (1) and (4) in the equatorial plane is extrapolated to a spherical grid (on Gauss collocation points) in the physical space. This is a straightforward process because u_s and u_ϕ are independent of z and u_z is a linear function of z. Then, the velocity field is expressed in spherical coordinates $(\mathbf{e_r},\mathbf{e}_\theta,\mathbf{e}_\phi)$ to compute the non linear induction term. The dimensionless equation of evolution of the magnetic field is:

$$\frac{\partial\mathbf{B}}{\partial t}=\nabla\times(\mathbf{u}\times\mathbf{B})+P_m^{-1}E\Delta\mathbf{B} \quad (5)$$

Changing the magnetic Prandtl number P_m changes directly the magnetic Reynolds number $R_\mathrm{m}=RePm=RoE^{-1}P_\mathrm{m}$ which is more commonly used in dynamo modeling. The induction equation is solved using spherical harmonics where the magnetic boundary conditions are easy to implement [9]. The induction part of the code has been checked using kinematic dynamo results [27] and the dynamo benchmark [28].

2.3. Numerical implementation

A finite difference scheme is used on an irregular radial grid (denser near the Stewartson layer) as well as on a regular radial grid (for the most turbulent cases). A semi implicit Crank–Nicholson scheme is used for linear terms in time whereas an Adams–Bashforth procedure is implemented for non linear terms. For low P_m, cylindrical and spherical radial grid steps may differ by a factor of 20, and time steps for the induction equation may be much longer than the velocity time steps (as much as 20 times).

For a run at $E=10^{-8}$, the stream function is computed on a cylindrical mesh made of 600 radial points and expanded in Fourier series up to degree $m=170$ in the azimuthal direction while the magnetic field is expanded in spherical harmonics ($L_\mathrm{max}=79$, $M_\mathrm{max}=32$) with an irregular radial grid of 150 points for $P_\mathrm{m}=10^{-2.5}$.

To compute the induction Eq. (5), the velocity field $(u_s,u_\phi,\overline{\frac{du_z}{dz}})$ is truncated in the Fourier space and computed back in physical space on a fine 2D equatorial grid. Knowing $\overline{\frac{du_z}{dz}}$, z-extrapolation is straightforward, and the velocity field is computed at each magnetic grid point using linear interpolation in the s-direction.

Convergence tests have been performed and are reported in Section 4.3.

3. Hydrodynamics

For low Rossby numbers, the split at the spherical boundary produces an internal shear layer in the fluid on a cylinder of radius R_s aligned with the rotation axis. This geostrophic viscous layer consists of two nested layers of different width as revealed by the asymptotic study of Stewartson [20] and illustrated later by a numerical study of Dormy et al. [21]; an $E^{1/4}$ thick layer accommodates the jump in the geostrophic azimuthal velocity and a narrower layer of size $E^{1/3}$, non-geostrophic, corresponds to an axial jet ensuring mass conservation.

In a previous study [23], we have presented the QG model, which can only reproduce only the $E^{1/4}$ layer, and we have studied the linear perturbations of this geostrophic internal viscous layer. It becomes unstable when the Rossby number exceeds a critical value Ro^c which varies as $\beta E^{1/2}$ [23]. At the onset, the instability is

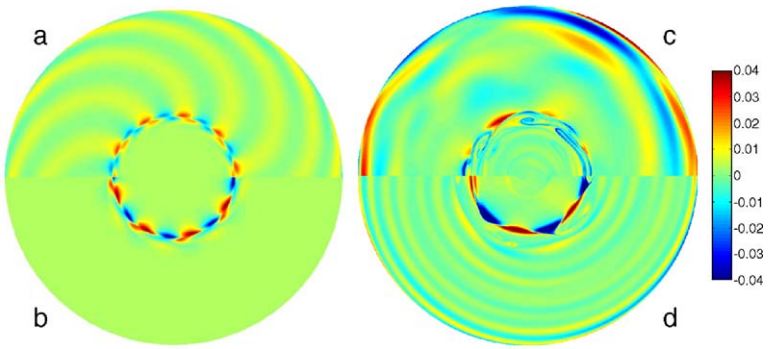

Fig. 2. z-vorticity maps in the equatorial plane. (a and b) $E=10^{-6}$, $Ro=0.0096$ and $Ro=-0.0111$, respectively. It shows the flow at the onset of hydrodynamic instabilities for both signs of the Rossby number. (c and d) $E=10^{-8}$, $Ro=0.02$ and $Ro=-0.02$, respectively. It shows a typical view of the "turbulent" regime for Rossby numbers about 30 times critical. The color bar gives the local vorticity scale for (c) and (d) only.

a Rossby wave, an azimuthal necklace of cyclones and anticyclones of size $E^{1/4}$ which propagates in the prograde direction as shown in Fig. 2a,b. Super rotation ($Ro>0$) generates a spiraling flow outside the shear layer while the flow is mainly located inside the shear layer for $Ro<0$. For supercritical Ro, the flow exhibits larger vortices (Fig. 2c,d) which are time-dependent but still drifting as Rossby waves. The flow stays mainly concentrated in the shear layer. Fig. 3 shows the kinetic energy spectra $E(k)$ of this QG turbulent flow. It is very steep: $E(k)\sim k^{-5}$, which is the slope predicted by Rhines [29] for turbulence in presence of Rossby waves [30]. This steep spectrum suggests that the small scales of the flow may be neglected in the induction equation.

Recently, in rotating turbulence experiments [31], it has been shown that for Rossby numbers up to 0.1 (regardless of how far above criticality) the velocity fluctuations recorded by hot-film probes are strongly correlated along the rotation axis direction, suggesting that a QG-model may describe such flows quite well.

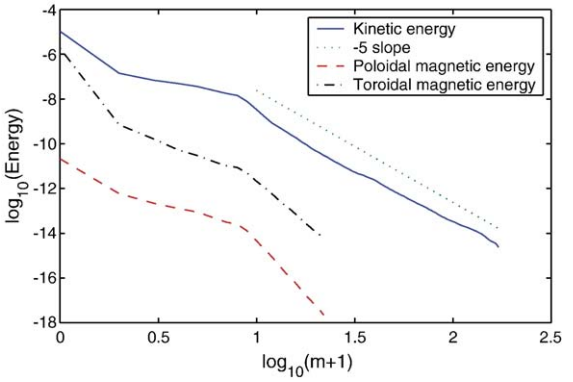

Fig. 3. Spectra of the kinetic energy, and both toroidal and poloidal magnetic energy for $E=10^{-8}$, $Ro=0.02$ (30 times critical) and $P_m=5\times10^{-3}$ (equivalent to $Re=2\times10^6$). The amplitude of the energy is arbitrary (linear calculation).

4. Dynamo action

For a given Ekman number ($E=10^{-6}$ to 10^{-8}) and a given Rossby number, Ro, from critical to a few times critical, we find the critical magnetic Prandtl number P_m of the onset of dynamo action by trial and error tests. As the flow is time-dependent, we detect dynamo criticality on long term time variations of the magnetic energy.

4.1. Overview of results

Unlike most kinematic dynamo models [32], a critical magnetic Prandtl number was found for every pair of dimensionless numbers (E, Ro) we have computed. In Fig. 4, the calculated critical magnetic Prandtl number P_m^c is plotted as a function of the Reynolds number $Re=Ro/E$. As expected, we found that an increase of the forcing (Ro) for a given E reduces the critical magnetic Prandtl number. A decrease of the critical magnetic Prandtl number is also observed as we lower the Ekman number. These two effects may be summarised by the use of the magnetic Reynolds number R_m. The data points in Fig. 4 are roughly compatible with the line $R_m=10^4$. However, the flow generates large deviations from this simple law of about a factor 3, which is quite small if you compare it to the variations of a few orders of magnitude of the dimensionless parameters E and Ro. We thus want to emphasize that the critical R_m remains roughly constant and seems to be independent of E and P_m.

The lowest critical magnetic Prandtl number (0.003) has been found for $E=10^{-8}$ and $Ro=0.02$. The critical magnetic Prandtl number is not independent of the sign of the differential rotation (sign of Ro). This is expected because the flow is quite different in the two cases as shown in Fig. 2. A negative differential rotation seems to lead to slightly lower dynamo thresholds.

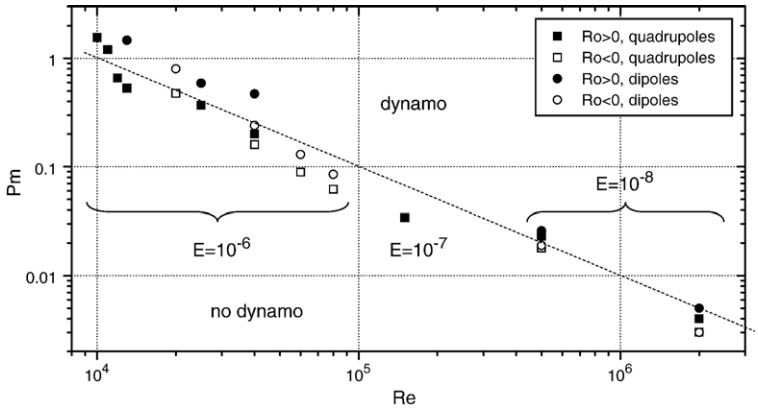

Fig. 4. Dynamo onset for different parameters: Critical magnetic Prandtl number P_m^c vs. the absolute Reynolds number $Re=|Ro|E^{-1}$. Dipole and quadrupole thresholds are respectively denoted by circles and squares while solid and open symbols represent positive and negative differential rotation. All the points lie around the $R_m=10^4$ line.

Antisymmetric axial velocities ($u_z(z)=-u_z(-z)$) and symmetric orthoaxial velocities ($u_{s,\phi}(z)=u_{s,\phi}(-z)$) generate two independent families of growing magnetic field in kinematic dynamos known as the dipole and quadrupole families [33]. The geometry of the two families are shown in Fig. 5a and b: the dipole family is dominated by an axial dipole, whereas the quadrupole family exhibits a strong axial quadrupole. Each family has a different critical magnetic Prandtl number. As shown in Fig. 4, we found that the dipole family has always a larger critical magnetic Reynolds number than the quadrupole family. This result is quite different from the conclusion of the work of Sarson and Busse [34]. Using Kumar and Roberts kinematic dynamos, they found that prograde spiraling of columns and prograde zonal flows favor dipole magnetic fields.

In both families, the strongest magnetic fields are produced in the Stewartson shear layer deep inside the sphere. The typical spectra given in Fig. 3 show that the computed magnetic fields are dominated by the toroidal axisymmetric component, which is about 100 times stronger than the non-axisymmetric features. At the surface of the sphere (Fig. 5c), the radial magnetic field is also mostly axisymmetrical, and the non-axisymmetric part is clearly associated to the geostrophic vortices produced in the Stewartson shear layer. An important fact is that decreasing E and P_m leaves the geometry of the growing magnetic field almost unchanged. This suggests that the details of dynamo action stay unaltered, because the flow itself remains also quite similar.

Fig. 6 compares the details of the magnetic field and the velocity field. We can see that due to the very low value

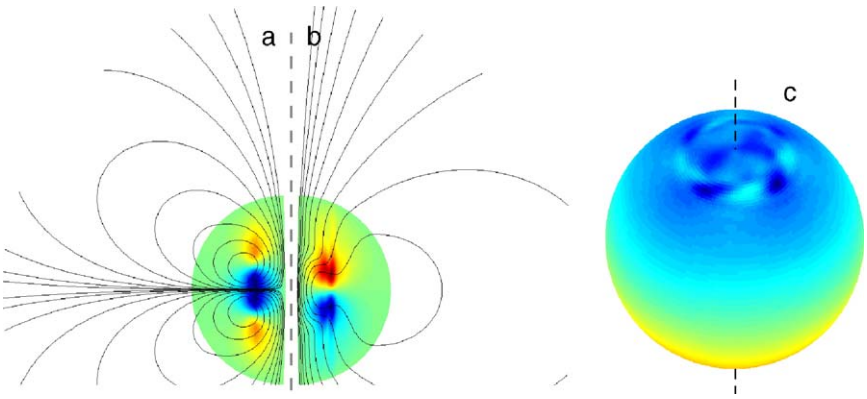

Fig. 5. Growing magnetic field in kinematic dynamos for $E=10^{-8}$. (a and b) Meridional cuts of the sphere showing the axisymmetric part of the magnetic field. The solid lines are the poloidal field lines and the color map represents the azimuthal field. Panel (a) shows a quadrupole field obtained at $Ro=0.02$ and $P_m=0.005$. Panel (b) shows a dipole field obtained at $Ro=-0.02$ and $P_m=0.003$ (the quadrupole family has been filtered out to compute the dipole family). Panel (c) is a spherical map of the radial magnetic field at the surface of the core, corresponding to case (b), the dashed line being the rotation axis. The corresponding vorticity fields are shown in Fig. 2c,d.

of P_m, the magnetic field does not follow the velocity field perfectly, although the main features of the flow are still present in the magnetic field. As a consequence of the Rossby-wave propagation, there is a systematic shift in the azimuthal direction between magnetic and velocity fields. We should also mention here that the small-scale structures of the flow are found to be unimportant for the dynamo action (see also Section 4.3).

The geometry of the magnetic field may be understood in term of Parker-Ω effects [33,9]. A very large toroidal magnetic field compatible with the azimuthal flow is converted to a poloidal magnetic field by the columnar flow through a Parker effect (also known as giant alpha effect). Any non-azimuthal component of the magnetic field is transformed into an azimuthal component by the strong differential rotation in the Stewartson layer by Ω effect.

The Ekman pumping may be important for the dynamo process: although the β-effect produces axial velocities, they are out of phase with the axial vorticity at the onset of thermal convection in a rapidly rotating annulus and cannot contribute to the mean helicity, whereas axial velocities due to Ekman pumping are in phase with the axial vorticity. However, the Ekman pumping flow is of order $E^{1/2}$, so that a dynamo process based on the Ekman pumping becomes very weak when lowering the Ekman number. In addition, when the Ekman pumping flow is artificially removed in our dynamo simulations, we still observe dynamo action with nearly the same threshold. Similar results have been obtained theoretically by Busse [35], who derived a geodynamo model based on thermal convection in which the dynamo process due to Ekman pumping vanishes at small E, while a β-effect mechanism takes over. We may thus conclude that the β-effect alone may produce an efficient Parker effect, without requiring an Ekman pumping flow.

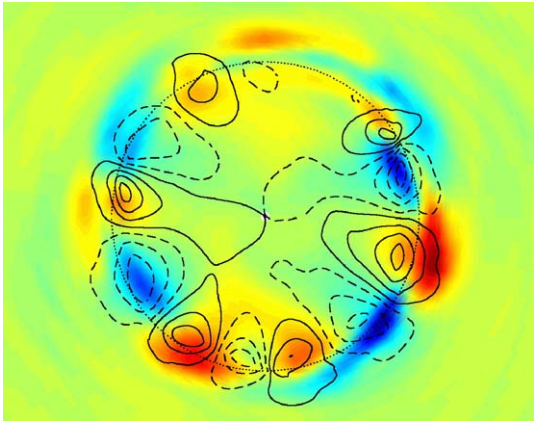

Fig. 6. Close-up of the radial magnetic field (color map) and the radial velocity field (contours) for $E=10^{-8}$, $Ro=-0.02$, $P_m=0.005$, in the equatorial plane. Red and blue are respectively outward and inward magnetic field, whereas solid and dashed lines are respectively positive (outward) and negative (inward) radial velocity field contours. The dotted line circle is the split radius ($r=0.35$).

Furthermore, we have not been able to find a critical magnetic Prandtl number with a steady flow (either a time averaged flow or a flow with its time evolution stopped at a given time). This implies that the time evolution of the flow is a key ingredient for dynamo action in these quasi-geostrophic dynamos. The propagation of Rossby waves is required so as to put in phase the non axisymmetric magnetic fields and velocities in order to produce an axisymmetric poloidal magnetic field. This type of Parker effect was proposed in the model of Braginsky [36].

Currently, many dynamo experiments are designed with the help of numerical simulations (kinematic dynamos). Even when the flow is highly turbulent ($Re>10^6$), mean flow approaches are used for simplicity to find the dynamo onset [1,37–39]. This method would fail in the case of Stewartson dynamos for which time dependence is required.

4.2. Oscillating solution

As in many $\alpha\Omega$ dynamos [33], we sometimes obtain a time oscillating solution for the Stewartson dynamo. Dipole solutions for $E=10^{-6}$ do exhibit such a behavior. The growth rate of one of these dynamos is plotted on Fig. 7, showing three time scales: the smallest one is the time scale of the velocity fluctuations. The intermediate time scale is the time needed for the growth rate to go from its minimum to its maximum value. The large time scale is the period of oscillation, unrelated to any time scale of the flow, and corresponds to a fraction of the magnetic diffusion time. The oscillation period shortens as the forcing is increased above the dynamo threshold.

In the context of kinematic dynamos, this behavior corresponds to a complex eigenvalue in the framework of linear stability [33,9,27]. Since our flow is time-dependent, the kinematic dynamo is not an eigenvalue-type problem. However, if the flow changes are much faster than any magnetic field variations, it is a good approximation. Hence, we consider here a toy model with two coupled magnetic modes B_1 and B_2. Let us assume that the induction equation can be approximated by the following system:

$$\frac{dB_1}{dt} = \lambda_1 B_1 + K_{12} B_2 \tag{6}$$

$$\frac{dB_2}{dt} = \lambda_2 B_2 - K_{21} B_1 \tag{7}$$

with real coefficient λ_1, λ_2, K_{12}, K_{21}. For a low coupling ($K_{12}K_{21}<(\lambda_1-\lambda_2)^2/2$) the eigenvalues of this system are real, so that the growing solution will be the combination of B_1 and B_2 corresponding to the highest eigenvalue. This is the case for the quadrupole family at $Ro<0$. However, when the coupling $K_{12}K_{21}$ is sufficiently strong, the eigenvalues are complex conjugate with a real part $\lambda_r=(\lambda_1+\lambda_2)/2$. As a result, the growing magnetic field oscillates periodically between B_1 and B_2 with a frequency increasing with the strength of the coupling. The parameters λ_1, λ_2, K_{12}, K_{21} can be adjusted in order to recover the curve

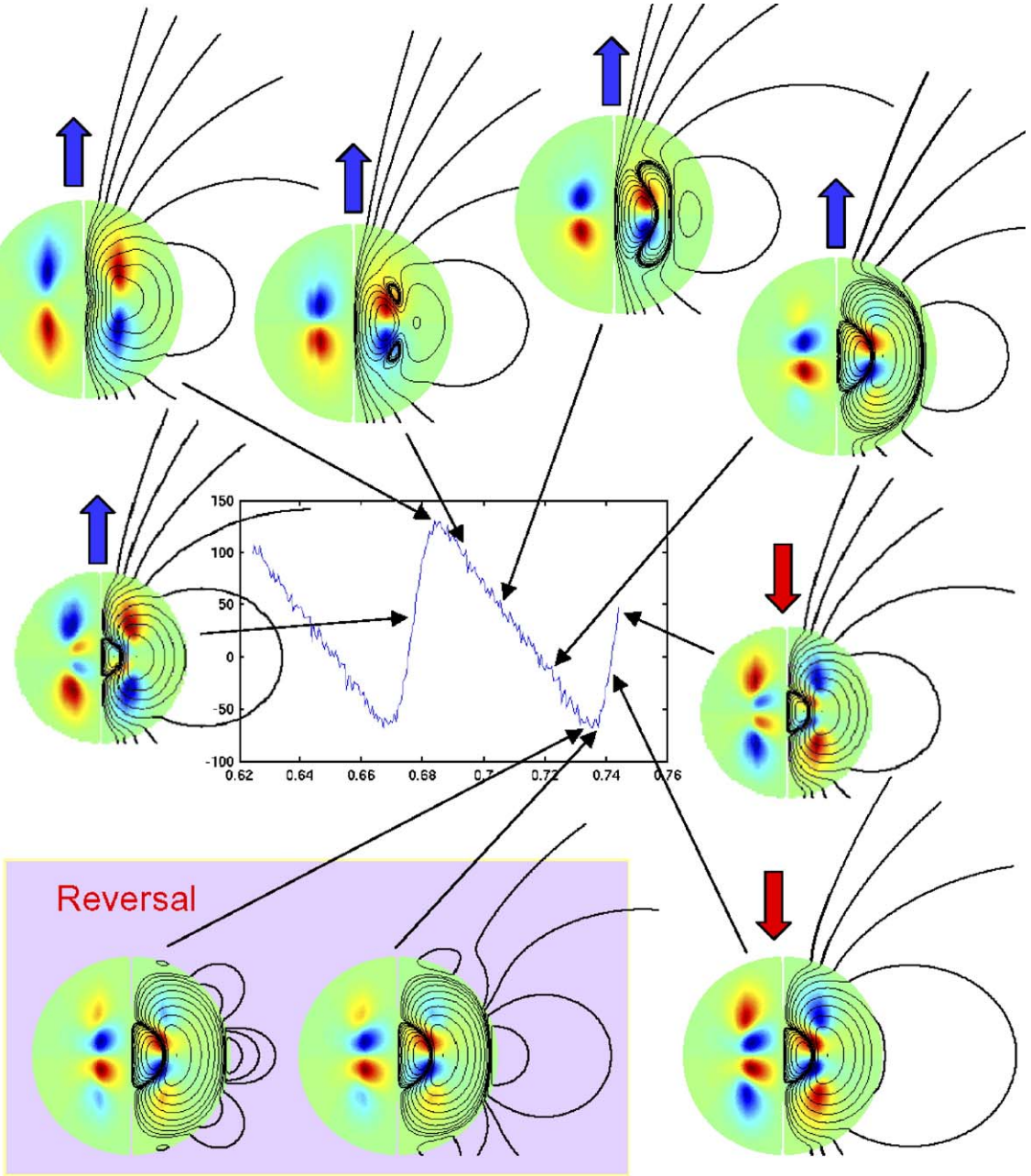

Fig. 7. Magnetic field reversal observed at $E=10^{-6}$, $Ro=-0.08$ and $P_m=0.1$. The graph shows the evolution of the growth rate of the magnetic energy as a function of time (in magnetic diffusion time units). Each snapshot shows the geometry of the magnetic field at different times in the same way as Fig. 5.

shown in Fig. 7 (without the small oscillations) when plotting the growth rate of the energy of such a system as a function of time. The intermediate time scale (time for the growth rate to go from its minimum to its maximum) is very close to the phase shift between B_1 and B_2, and one of the two modes is dominant near the minimum of the growth rate cycle, while the other one is dominant near the maximum, with growth rates close to λ_1 and λ_2.

The reversal process at work in our simulations is a smooth periodic evolution of the magnetic field, but at the surface it takes the form of a sudden sign reversal. In fact, a reversed poloidal magnetic field is slowly growing inside the Stewartson layer, pushing away the initial poloidal magnetic field until it reaches the outer boundary. Then, the reversed dipole magnetic field suddenly appears at the surface and ultimately the poloidal field reverses at the center. During the oscillation, the axisymmetric toroidal magnetic field patches in the Stewartson layer migrate toward the equator as reversed polarity toroidal fields are formed at high latitudes. This migration could be understood in terms of Parker dynamo waves [40,33].

4.3. Impact of truncation

To check if such strong truncations that completely neglect the small scales of the flow for the induction processes are valid, we tested several of our truncated calculations by increasing $M_{\max}$ and reducing the time step. We saw no significant differences. Some of these runs, that demonstrate the convergence of our results, are shown in Table 1. Furthermore, there is no significant difference between the temporal evolution of the growth rate in the time series shown in Fig. 8.

Table 1
Effect of the truncation of the magnetic field model on the growth rate

E	Ro	P_m	N_R^U	m_{max}^U	N_R^B	m_{max}^B	l_{max}^B	dt^U	dt^B	gr
10^{-6}	0.04	0.3	400	64	100	64	64	0.1	0.1	45.72
10^{-6}	0.04	0.3	400	64	100	16	59	0.1	0.6	45.68
10^{-6}	−0.08	0.1	400	64	200	42	79	0.05	0.2	30
10^{-6}	−0.08	0.1	400	64	100	21	59	0.05	0.3	31

N_R is the number of radial grid-points; m_{max} is the number of azimuthal Fourier mode; l_{max} the highest order of the spherical harmonics; dt is the time stepping (based on the rotation rate); gr is the growth rate of the magnetic energy. Superscript 'U' or 'B' denotes a quantity relative to the velocity field or to the magnetic field models.

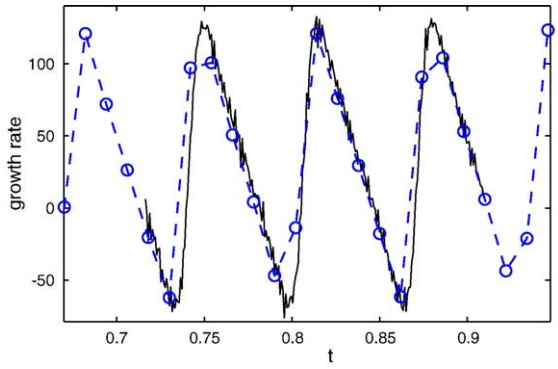

Fig. 8. Growth rate of the magnetic energy at $E=10^{-6}$, $Ro=-0.08$, $P_m=0.1$ and two different resolutions (given in Table 1). The dashed line is the less resolved calculation (in both space and time domains), and the continuous line is the high resolution one.

These tests clearly show that the scale-separation hypothesis in both space and time is, as expected, valid for such small values of P_m.

5. Conclusion

In summary, we have computed a quasi-geostrophic dynamo based on a Stewartson shear layer flow. The scale separation approach works because the small scales of the flow in our rotating sphere are negligible (very steep kinetic energy spectrum $E(k)\sim k^{-5}$). Our preliminary results may be interpreted in terms of a Parker-Ω dynamo. The Ω effect is generated by the shear of the Stewartson layer itself whereas the Parker effect is produced by vortices associated with the Rossby waves due to the instability of the shear layer. These understandings are very encouraging for our ongoing experimental modeling of the geodynamo. As described in Cardin et al. [24], we are building a spherical Couette experiment using liquid sodium which may validate and enlarge our present numerical findings.

For the first time, we have computed a spherical dynamo with a very low magnetic Prandtl number ($<10^{-2}$) and a very low Ekman number (10^{-8}) (corresponding to a very high Reynolds number $Re>10^6$). The critical magnetic Reynolds number seems to be quite independent of the Ekman and magnetic Prandtl numbers. Even though our dimensionless parameters stay far away from parameters of planetary cores, our calculations use dimensionless numbers which are in the correct asymptotic regime for the modeling of the geodynamo. The key ingredients of our approach is to take into account a specific property of the rotating fluid, quasi-

geostrophy, which allows us to use a 2D model to compute the flow evolution, and the separation of scales between the magnetic field and the velocity field, allowing us to use a coarse 3D mesh for the magnetic field.

Concerning the dependence on P_m, our results are compatible with the results of Ponty et al. for turbulent Taylor Green flow [41] while they contradict those of Schekochihin et al. showing an inhibition of dynamo action as P_m is decreased [42]. In the geophysical context, the study of Christensen and coworkers suggested that by decreasing the Ekman number, the magnetic Prandtl number could be decreased as well without looszing dynamo action. This suggestion was based on 3D simulations, varying the Ekman number by a factor of 3 [7]. By varying both parameters by a factor of 100 (see Fig. 4), the present study clearly confirms this idea, which has very important geophysical implications, showing a possible link between the regime of existing numerical models and the regime of interest for the Earth.

We also showed that in the case studied in this paper, the mean flow or the static flow fails to produce a dynamo while the fully resolved time-dependent flow is successful. Indeed, time evolution of the flow and β effect are key ingredients for dynamo action in our models, while Ekman pumping can be neglected without losing the dynamo effect.

The next step will be to add the Lorentz force in the QG equation to compute saturated dynamos. One of the difficulties is to compute the action of the large-scale magnetic field on the small-scale motions of the fluid. Preliminary results are encouraging and exhibit saturated dynamos very close to the kinematic dynamos described here. A comparison with 3D calculations would also be very interesting and 3D preliminary results of J. Wicht (private communication) seem to confirm our results.

A quasi-geostrophic approach might also be used to build thermal convective dynamos. A zonal geostrophic flow is produced by the Reynolds stresses associated to the thermal columns [18,43] but its amplitude is much lower compared to the differential rotation imposed in the Stewartson problem. Would it be enough to start a Stewartson dynamo type? for what forcing? Would it work for very low Ekman and magnetic Prandtl numbers?

Acknowledgements

Calculations were performed at SCCI (Observatoire de Grenoble) and at IDRIS (CNRS). This work has been supported by the programme "DyETI" of CNRS/INSU. We wish to thank Henri-Claude Nataf, Thierry Alboussière, Emmanuel Dormy and the reviewers for useful comments.

References

[1] A. Gailitis, O. Lielausis, E. Platacis, S. Dementév, A. Cifersons, G. Gerbeth, Th. Gundrum, F. Stefani, M. Christen, G. Will, Magnetic field saturation in the Riga dynamo experiment, Phys. Rev. Lett. 86 (2001) 3024–3027.
[2] R. Stieglitz, U. Müller, Experimental demonstration of a homogeneous two-scale dynamo, Phys. Fluids 13 (2001) 561–564.
[3] P. Cardin, D. Brito. Survey of experimental dynamos, Presse Universitaire de Grenoble, (in press).
[4] G. Glatzmaier, P. Roberts, A three-dimensional self-consistent computer simulation of a geomagnetic field reversal, Nature 377 (1995) 203.
[5] A. Kageyama, T. Sato, Generation mechanism of a dipole field by a magnetohydrodynamic dynamo, Phys. Rev. E 55 (1997) 4.
[6] W. Kuang, J. Bloxham, A numerical dynamo model in an earth-like dynamical regime, Nature 389 (1997) 371–374.
[7] U. Christensen, P. Olson, G. Glatzmaier, Numerical modelling of the geodynamo: a systematic parameter study, Geophys. J. Int. 138 (1999) 393.
[8] R.F. Gans, On hydromagnetic precession in a cylinder, J. Fluid Mech. 45 (1971) 111–130.
[9] D. Gubbins, P. Roberts, Geomagnetism, vol. 2, Jacobs J.A., 1987.
[10] E. Dormy, J.-P. Valet, V. Courtillot, Numerical models of the geodynamo and observational constraints, G-cubed 1 (2000) 62.
[11] M. Kono, P. Roberts, Recent geodynamo simulations and observations of the geomagnetic field, Rev. Geophys. 40 (2002) 1013.
[12] H.P. Greenspan, The theory of rotating fluids, Cambridge University Press, 1968.
[13] J.-P. Poirier, Physical properties of the earth's core, C. R. Acad. Sci. Paris 318 (1994) 341–350.
[14] F.H. Busse, Thermal instabilities in rapidly rotating systems, J. Fluid Mech. 44 (1970) 441–460.
[15] P. Cardin, P. Olson, Chaotic thermal convection in a rapidly rotating spherical shell: consequences for flow in the outer core, Phys. Earth Planet. Inter. 82 (1994) 235.
[16] J. Aubert, N. Gillet, P. Cardin, Quasigeostrophic models of convection in rotating spherical shells, G-cubed 4 (2003) 1052, doi: 10.1029/2002GC000456.
[17] E. Dormy, A. Soward, C. Jones, D. Jault, P. Cardin, The onset of thermal convection in rotating spherical shells, J. Fluid Mech. 501 (2004) 43–70.
[18] J. Aubert, D. Brito, H.-C. Nataf, P. Cardin, J.-P. Masson, A systematic experimental study of spherical shell convection in water and liquid gallium, Phys. Earth Planet. Inter. 128 (2001) 51–74.
[19] Y. Ponty, J.-F. Pinton, H. Politano, Simulation of induction at low magnetic Prandtl number, Phys. Rev. Lett. 92 (2004) 144503.
[20] K. Stewartson, On almost rigid rotations, J. Fluid Mech. 26 (1966) 131.
[21] E. Dormy, P. Cardin, D. Jault, Mhd flow in a slightly differentially rotating spherical shell, with conducting inner core, in a dipolar magnetic field, Earth Planet. Sci. Lett. 160 (1998) 15.
[22] R. Hollerbach, Instabilities of the Stewartson layer: Part 1. The dependence on the sign of *Ro*, J. Fluid Mech. 492 (2003) 289–302.
[23] N. Schaeffer, P. Cardin, Quasi-geostrophic model of the instabilities of the Stewartson layer, Phys. Fluids 17 (2005) 104111.
[24] P. Cardin, D. Brito, D. Jault, H.-C. Nataf, J.-P. Masson, Towards a rapidly rotating liquid sodium dynamo experiment, Magnetohydrodynamics 38 (2002) 177.

[25] H.-C. Nataf, T. Alboussière, D. Brito, P. Cardin, N. Gagnière, D. Jault, J.-P. Masson, D. Schmitt, Experimental study of super-rotation in a magnetostrophic spherical Couette flow. Geophys. and Astrophys. Fluid Dyn., in press.
[26] E. Plaut, F.H. Busse, Low-Prandtl-number convection in a rotating cylindrical annulus, J. Fluid Mech. 464 (August 2002) 345–363.
[27] M. Dudley, R. James, Time-dependent kinematic dynamos with stationary flows, Proc. R. Soc., Lond. A 425 (1989) 407–429.
[28] U.R. Christensen, J. Aubert, P. Cardin, E. Dormy, S. Gibbons, G.A. Glatzmaier, E. Grote, Y. Honkura, C. Jones, M. Kono, M. Matsushima, A. Sakuraba, F. Takahashi, A. Tilgner, J. Wicht, K. Zhang, A numerical dynamo benchmark, Phys. Earth Planet. Inter. 128 (2001) 51.
[29] P.B. Rhines, Waves and turbulence on a beta-plane, J. Fluid Mech. 69 (1975) 417–443.
[30] N. Schaeffer, P. Cardin, Rossby-wave turbulence in a rapidly rotating sphere, Nonlinear Process. Geophys. 12 (2005) 947–953.
[31] C.N. Baroud, B.B. Plapp, Z.-S. She, H.L. Swinney, Scaling in three-dimensional and quasi-two-dimensional rotating turbulent flows, Phys. Fluids 15 (2003) 2091–2104.
[32] D. Gubbins, C.N. Barber, S. Gibbons, J.J. Love, Kinematic dynamo action in a sphere: i). Effects of differential rotation and meridional circulation on solutions with axial dipole symmetry, Proc. R. Soc. Lond., A 456 (2000) 1333–1353.
[33] P.H. Roberts, Kinematic dynamo models, Philos. Trans. R. Soc. Lond., A 272 (1972) 663–698.
[34] G.R. Sarson, F.H. Busse, The kinematic dynamo action of spiralling convective flows, Geophys. J. Int. 133 (1998) 140–158.
[35] F.H. Busse, A model of geodynamo, Geophys. J. R. Astron. 42 (1975) 437–459.
[36] S.I. Braginsky, Self excitation of a magnetic field during the motion of a highly conducting fluid, Sov. Phys. JETP 20 (1964) 726–735.
[37] A. Tilgner, Numerical simulation of the onset of dynamo action in an experimental two-scale dynamo, Phys. fluids 14 (2002) 4092–4094.
[38] W. Dobler, P. Frick, R. Stepanov, Screw dynamo in a time-dependent pipe flow, Phys. Rev., E 67 (2003) 056309.
[39] L. Marié, J. Burguete, F. Daviaud, J. Léorat, Numerical study of homogeneous dynamo based on experimental von krmn type flows, Eur. Phys. J., B Cond. Matter Phys. 33 (2003) 469–485.
[40] E.N. Parker, Hydromagnetic dynamo models, Astrophys. J. 122 (1955) 293.
[41] Y. Ponty, P.D. Mininni, D.C. Montgomery, J.-F. Pinton, H. Politano, A. Pouquet, Numerical study of dynamo action at low magnetic Prandtl numbers, Phys. Rev. Lett. 94 (2005) 164502.
[42] A.A. Schekochihin, S.C. Cowley, J.L. Maron, J.C. McWilliams, Critical magnetic Prandtl number for small-scale dynamo, Phys. Rev. Lett. 92 (2004) 054502.
[43] U.R. Christensen, Zonal flow driven by strongly supercritical convection in rotating spherical shells, J. Fluid Mech. 470 (2002) 115–133.